

Superhard Monoclinic Polymorph of Carbon

Quan Li,¹ Yanming Ma,^{1,*} Artem R. Oganov,^{2,3,†} Hongbo Wang,¹ Hui Wang,¹ Ying Xu,¹
Tian Cui,¹ Ho-Kwang Mao,^{4,‡} and Guangtian Zou¹

¹State Key Lab of Superhard Materials, Jilin University, Changchun 130012, China

²Department of Geosciences and New York Center for Computational Science, Stony Brook University,
Stony Brook, New York 11794, USA

³Department of Geology, Moscow State University, 119899 Moscow, Russia

⁴Geophysical Laboratory, Carnegie Institution of Washington, 5251 Broad Branch Road NW, Washington, D.C. 20015-1305, USA

(Received 30 December 2008; published 29 April 2009)

We report a novel phase of carbon possessing a monoclinic $C2/m$ structure (8 atoms/cell) identified using an *ab initio* evolutionary structural search. This polymorph, which we call *M*-carbon, is related to the (2×1) reconstruction of the (111) surface of diamond and can also be viewed as a distorted (through sliding and buckling of the sheets) form of graphite. It is stable over cold-compressed graphite above 13.4 GPa. The simulated x-ray diffraction pattern and near *K*-edge spectroscopy are in satisfactory agreement with the experimental data [W.L. Mao *et al.*, *Science* **302**, 425 (2003)] on overcompressed graphite. The hardness and bulk modulus of this new carbon polymorph are calculated to be 83.1 and 431.2 GPa, respectively, which are comparable to those of diamond.

DOI: 10.1103/PhysRevLett.102.175506

PACS numbers: 61.50.Ks, 61.66.Bi, 62.50.-p

Carbon can adopt a wide range of structures, such as graphite, diamond, hexagonal diamond (lonsdaleite), carbynes, nanotubes, fullerenes, and amorphous carbon. This is because of carbon's ability to form sp -, sp^2 -, and sp^3 -hybridized bonds [1]. The conversion mechanisms between various forms of carbon have long been a topic of interest since these polymorphs have large differences in both electronic and mechanical properties. Without the use of catalysts, graphite can convert to diamond at pressures above 15 GPa but at very high temperatures (1600–2500 K) [2,3]. On the other hand, by applying pressure to graphite at room temperature, a structural phase transition occurs above 14 GPa as characterized by the obvious changes in the electrical resistivity [4,5], optical reflectivity and transmittance [6–8], Raman modes [6,9,10], x-ray diffraction (XRD) pattern [11–13], hardness [13], and the near *K*-edge spectroscopy [13]. Remarkably, this new phase of carbon is superhard as evidenced by the broadening of ruby fluorescence lines and its ability to indent diamond anvils [13]. However, the crystal structure of this cold-compressed postgraphite polymorph remains unknown. It was initially thought to be hexagonal diamond, an intermediate phase between graphite and diamond, or an amorphous phase [1,12,14,15]. However, no Raman bands are observed in the 1330 cm^{-1} frequency region characteristic of hexagonal/cubic diamonds [10], and recently measured hydrostatic XRD patterns have revealed that Bragg peaks persisted and remained traceable to the original graphite pattern, ruling out the possibility of amorphous carbon [13]. Very recently, a series of honeycomb lattices composed of a mixture of sp^2 and sp^3 bonds were proposed as the structural candidates [16], but none of them can account for the experimental XRD [13]. Here we have

extensively explored the crystal structures of carbon in a wide pressure range (0–100 GPa) using the newly developed evolutionary algorithm in crystal structure prediction [17–19]. Besides diamond and hexagonal diamond, we have uncovered a novel monoclinic structure with $C2/m$ symmetry as a metastable low-energy polymorph that is more favorable than graphite above 13.4 GPa. We call this monoclinic polymorph *M*-carbon. Remarkably, the simulated XRD patterns and energy-loss near-edge spectroscopy (ELNES) are in satisfactory agreement with the experimental observation [13]. Most strikingly, this new polymorph has a high hardness (83 GPa) comparable to that of diamond.

An *ab initio* evolutionary algorithm [17–19], designed to search for the structure possessing the lowest free energy, has been employed. The most significant feature of this methodology is the capability of predicting the stable structure at given pressure and temperature conditions with only the knowledge of the *chemical composition*. The details of the search algorithm and its first several applications have been described elsewhere [17–22]. On the way to the global minimum, this algorithm gradually focuses a search on the most promising areas of the (free) energy landscape, thus giving an enhanced (though not exhaustive) sampling of low-energy structures. The underlying structure relaxations were performed using density functional theory within the local density approximation (LDA) as implemented in the Vienna *ab initio* simulation package VASP code [23]. The all-electron projector-augmented wave method [24] was adopted with $2s^2 2p^2$ treated as valence electrons. A plane-wave basis set with an energy cutoff of 1000 eV was used and gave well converged total energies (~ 1 meV/atom). The phonon fre-

quencies for *M*-carbon were calculated using the direct supercell method, which uses the forces obtained by the Hellmann-Feynman theorem calculated from the optimized supercell (64 atoms). The ELNES is calculated by using the all-electron full potential linearized augmented plane-wave (FP-LAPW) method [25]. Since a hole in the core orbital of the excited atom has an important influence on the density of states and then on the ELNES, Slater's transition state method [26] is used to simulate the core-hole effect. In order to avoid the interactions between adjacent core holes, a supercell containing 64 atoms for both graphite and monoclinic *C2/m* carbon is employed. Convergence tests gave the choice of a 2000 *k*-point set for graphite and a 50 *k*-point set for *M*-carbon in supercell calculations. A Gaussian contribution of 0.5 eV FWHM Gaussian is taken into account in the instrumental line broadening. The Mulliken bond population is calculated using the pseudopotential plane-wave technique [27].

We performed variable-cell structure prediction simulations using the above evolutionary methodology for carbon containing two, four, six, and eight atoms in the simulation cell at 10, 15, 30, and 100 GPa, respectively. Besides cubic and hexagonal diamond, our simulations revealed a monoclinic structure with *C2/m* symmetry as depicted in Figs. 1(a) and 1(b). Within this structure, four inequivalent atoms occupy the crystallographic $4i$ site in the unit cell.

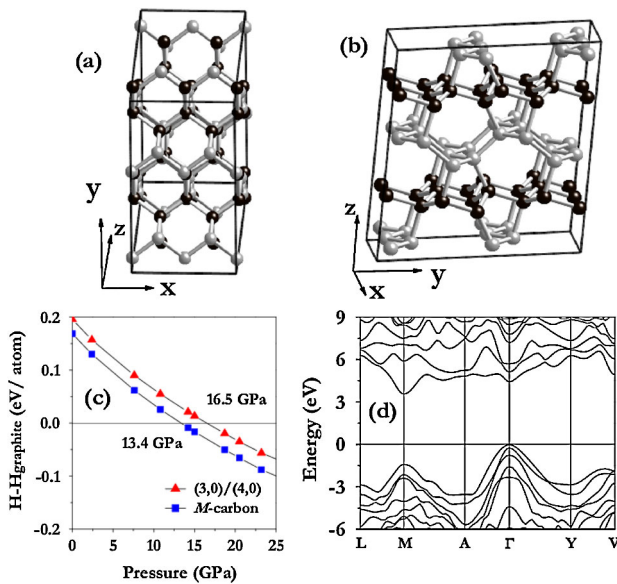


FIG. 1 (color online). (a),(b) Polyhedral views of the crystal structure of *M*-carbon. The gray (black) spheres represent the different warped layers. At zero pressure, lattice parameters of *M*-carbon are $a = 9.089 \text{ \AA}$, $b = 2.496 \text{ \AA}$, $c = 4.104 \text{ \AA}$, and $\beta = 96.96^\circ$ with four inequivalent crystallographic sites, occupying the $4i$ (0.4428, 0.5, 0.1206), (0.4419, 0, 0.3467), (0.2858, 0.5, 0.9406), and (0.2715, 0, 0.4149) positions, respectively. (c) The enthalpies per atom of (3, 0)/(4, 0) and *M*-carbon as a function of pressure with respect to graphite. (d) Calculated electronic band structure of *M*-carbon at 15 GPa.

The crystal is made of exclusively three-dimensional sp^3 hybridized covalent bonds, just as in the well-known (2×1) reconstruction of the (111) surface of diamond and silicon. Interestingly, since *M*-carbon presents sixfold rings forming warped “layers,” this intriguing structure can be understood as distorted graphite. Upon compression on graphite, sliding and buckling of the planes are accompanied by the formations of sp^3 bonds connecting the planes. Enthalpy calculations [Fig. 1(c)] suggest that *M*-carbon is energetically much more stable than the previously proposed (3, 0)/(4, 0) structure which has the lowest enthalpy among several hybrid diamond-graphite structures [16]. The predicted graphite \rightarrow *M*-carbon transition pressure is 13.4 GPa, which is in excellent agreement with the changes at ~ 14 GPa in the experimental XRD patterns [11–13]. The *M*-carbon structure is also consistent with the experimental suggestion that cold-compressed graphite should have either orthorhombic or monoclinic symmetry [13]. Furthermore, to confirm the dynamical stability of *M*-carbon, we have calculated its phonon dispersion curves. No imaginary frequencies were observed throughout the whole Brillouin zone, indicating that *M*-carbon is dynamically stable.

The theoretical total energies as a function of volume of *M*-carbon, diamond, and *c*-BN are fitted to the third-order Birch-Murnaghan equation of state to obtain the bulk modulus (B_0), as listed in Table I. Strikingly, the predicted B_0 of *M*-carbon (431.2 GPa) sits in between the two best superhard materials—*c*-BN (401.2 GPa) and diamond (468.5 GPa). We have estimated the intrinsic hardnesses of these three materials using the Šimůnek model [32]. This calculation correctly reproduces the experimental hardness of *c*-BN and diamond (Table I). Remarkably, the predicted hardness for *M*-carbon is 83.1 GPa, which is much higher than that of *c*-BN (62.4 GPa) and comparable to that of diamond (94.4 GPa). The predicted high bulk modulus and hardness present a natural explanation on the experimental observation that the cold-compressed

TABLE I. Calculated volume (V), bulk modulus (B_0), and hardness (H) for graphite, diamond, *c*-BN, and *M*-carbon at zero pressure.

Materials	Methods	V [$(\text{\AA}^3/\text{atom})$]	B_0 (GPa)	H (GPa)
Graphite	This work	8.47	31.0	
	Expt.	8.78 ^a	33.8 ^a	
Diamond	This work	5.52	468.5	94.4
	Expt.	5.68 ^b	446 ^b	60–120 ^c
<i>c</i> -BN	This work	5.75	401.2	62.4
	Expt.	5.91 ^d	387 ^d	47 ^e
<i>M</i> -carbon	This work	5.78	431.2	83.1

^aReference [9].

^bReference [28].

^cReference [29].

^dReference [30].

^eReference [31].

graphite sample left a “ring crack” on the diamond anvils cell [13]. In the quest for the origin of the high hardness in *M*-carbon, we have applied a Mulliken analysis to estimate the strength of covalent bonds. It is found that the Mulliken overlap population of sp^3 C-C bonds in *M*-carbon is in the range of 0.67–0.84, comparable to that (0.75) of diamond.

It is known that ELNES is a powerful technique, particularly well suited for obtaining local chemical composition and chemical bonding information in light element materials. Figure 2 shows the simulated carbon *K*-edge spectra along the *c* axis together with experimental spectra. The calculated results at 2.4 and 10.8 GPa for graphite agree well with the experimental data. We have successfully reproduced the increased intensity of π^* peak ($1s$ to π^* transitions) in graphite on compression. Note that the theoretical intensity in the energy region above 300 eV is weaker than the experimental data, which is understandable since the standard LAPW basis set is insufficient with respect to the continuum states [33], but the LAPW method is very successful near the threshold on which we are focusing. It is clear that pure *M*-carbon with exclusively sp^3 hybridization has no π bonding feature. However, it is experimentally observed that the π^* component in the near *K*-edge spectrum gradually dropped above the transition and remains up to 23 GPa [13]. We have thus proposed that the cold-compressed graphite experimentally prepared in Ref. [13] is actually a mixture of graphite and *M*-carbon. With the mixed structural models, the experimental peak positions, shapes, and reduced intensity of the π^* peak with pressure are well reproduced by theory [Figs. 2(b) and 2(c)]. The experimental spectra are understandable since

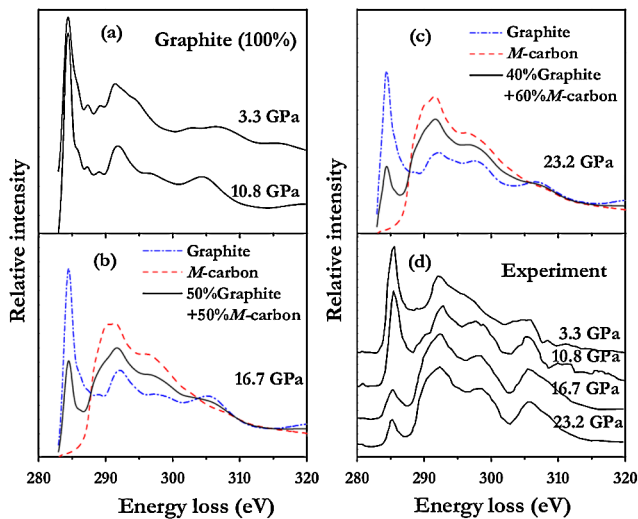


FIG. 2 (color online). Theoretical carbon *K*-edge spectra for pure graphite (a) and the mixture of *M*-carbon and graphite with different weights: 50% graphite + 50% *M*-carbon (b) and 40% graphite + 60% *M*-carbon (c). (d) Experimental data from Ref. [13]. Calculated results have been shifted and aligned to facilitate comparison with experiment.

the formation of the sp^3 bonds in *M*-carbon occurs at the expense of the π bonding within the graphene sheets.

To further confirm our structural model, we have simulated the XRD patterns to compare with the experimental data (Fig. 3). At both 3.3 and 13.7 GPa, the simulated intensive peak positions and relative intensities of graphite match the experimental observation very well. Carbon is a light material with a small scattering cross section. This gives carbon a challenging material for the XRD measurement and results in the failure of the observation of the weaker peaks in graphite ranging from 11° to 14° due to the strong background intensity (Fig. 3). Above the transition, as carbon atoms between graphite layers pair and form σ bonds, the in-plane reflections 100 and 110 broaden significantly and became intense relative to others. Significantly, XRD of *M*-carbon correctly reproduces the major experimental findings [12,13] that the strongest line of the high pressure phase appears in between the 100 and 110 peaks. With increasing pressure, the diffraction peaks from *M*-carbon become prominent. Note that, similar to that in pure graphite, the relatively weaker peaks of *M*-carbon in the range of 11° – 14° have also merged into the background, and those peaks at $\sim 9^\circ$ and $\sim 17^\circ$ contributed to the peak broadening (Fig. 3). Analysis of the

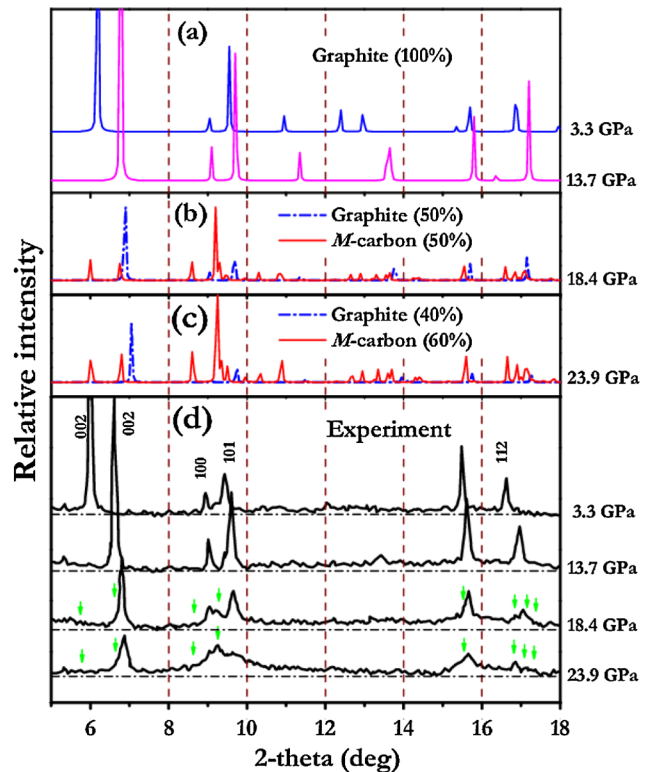


FIG. 3 (color online). The simulated XRD patterns of pure graphite (a) and the mixture of graphite and *M*-carbon with different weights (b),(c). (d) The experimental XRD patterns from Ref. [13]. The used x-ray wavelength is 0.3329 \AA as employed in the experiment [13]. Arrows stand for those XRD peaks of *M*-carbon observed by experiments.

XRD patterns thus provides further confirmation that *M*-carbon is formed upon cold compression of graphite.

The electronic band structure calculations reveal that *M*-carbon is a wide gap insulator with an indirect band gap of 3.6 eV [Fig. 1(d)]. Because of the well-known band gap underestimation in LDA, the true energy gap of *M*-carbon should be even larger. This naturally explains the experimental observations of optical transparency, a sharp drop in optical reflectivity, and an increase in optical transmittance of the compressed graphite beyond the transition [6–8]. To be optically transparent, the new phase has to have a band gap of at least 1.8 eV and at least 3 eV to be colorless. The coexistence of graphite with *M*-carbon explains a recent electrical measurement [5] that shows a small increase in electrical resistivity above 20 GPa, though the sample remained conducting throughout the pressure range of 0–48 GPa due to the residual presence of conductive graphite.

In conclusion, an *ab initio* evolutionary algorithm in crystal structure prediction was employed to reveal a likely candidate for cold-compressed postgraphite, *M*-carbon. *M*-carbon is stable over cold-compressed graphite above 13.4 GPa, which is in good agreement with the experimental observation. This polymorph possesses high hardness (83.1 GPa) and bulk modulus (431.2 GPa), which are comparable to those of diamond. The experimentally observed changes in XRD, near *K*-edge spectroscopy, and electrical resistance of cold-compressed graphite at the phase transition are explained by the coexistence of *M*-carbon and graphite. At low temperatures, compression of graphite produces *M*-carbon (rather than diamond) because of the structural relationship between these two phases, implying relatively easy transformation kinetics.

We are thankful for financial support from the NSAF of China under Grant No. 10676011, the National Natural Science Foundation of China under Grant No. 10874054, the China 973 Program under Grant No. 2005CB724400, the Program for 2005 New Century Excellent Talents in University, and the 2007 Cheung Kong Scholars Program of China. Use of the HPCAT x-ray facility was supported by DOE-BES, DOE-NNSA-CDAC, NSF, and the W.M. Keck Foundation

*Corresponding authors.

mym@jlu.edu.cn

†aoganov@notes.cc.sunysb.edu

‡h.mao@gl.ciw.edu

- [1] E.D. Miller, D.C. Nesting, and J.V. Badding, *Chem. Mater.* **9**, 18 (1997).
- [2] H. Sumiya and T. Irifune, *J. Mater. Res.* **22**, 2345 (2007).
- [3] T. Irifune *et al.*, *Nature (London)* **421**, 806 (2003).
- [4] E.P. Bundy and J.S. Kasper, *J. Chem. Phys.* **46**, 3437 (1967).
- [5] J.R. Patterson *et al.*, *Phys. Rev. Lett.* **85**, 5364 (2000).
- [6] A.F. Goncharov, I.N. Makarenko, and S.M. Stishov, *Sov. Phys. JETP* **69**, 380 (1989).
- [7] M. Hanfland, K. Syassen, and R. Sonnenschein, *Phys. Rev. B* **40**, 1951 (1989).
- [8] W. Utsumi and T. Yagi, *Science* **252**, 1542 (1991).
- [9] M. Hanfland, H. Beister, and K. Syassen, *Phys. Rev. B* **39**, 12 598 (1989).
- [10] J. Xu, H.K. Mao, and R.J. Hemley, *J. Phys. Condens. Matter* **14**, 11 549 (2002).
- [11] Y. Zhao and I.L. Spain, *Phys. Rev. B* **40**, 993 (1989).
- [12] T. Yagi *et al.*, *Phys. Rev. B* **46**, 6031 (1992).
- [13] W.L. Mao *et al.*, *Science* **302**, 425 (2003).
- [14] A.F. Goncharov, *High Press. Res.* **8**, 607 (1992).
- [15] F.P. Bundy *et al.*, *Carbon* **34**, 141 (1996).
- [16] F.J. Ribeiro *et al.*, *Phys. Rev. B* **72**, 214109 (2005).
- [17] A.R. Oganov, C.W. Glass, and S. Ono, *Earth Planet. Sci. Lett.* **241**, 95 (2006).
- [18] A.R. Oganov and C.W. Glass, *J. Chem. Phys.* **124**, 244704 (2006).
- [19] C.W. Glass, A.R. Oganov, and N. Hansen, *Comput. Phys. Commun.* **175**, 713 (2006).
- [20] Y. Ma, A.R. Oganov, and C.W. Glass, *Phys. Rev. B* **76**, 064101 (2007).
- [21] Y. Ma, A.R. Oganov, and Y. Xie, *Phys. Rev. B* **78**, 014102 (2008).
- [22] G. Gao *et al.*, *Phys. Rev. Lett.* **101**, 107002 (2008).
- [23] G. Kresse and J. Furthmüller, *Phys. Rev. B* **54**, 11 169 (1996).
- [24] P.E. Blöchl, *Phys. Rev. B* **50**, 17 953 (1994).
- [25] P. Blaha *et al.*, *WIEN2K, An Augmented-Plane-Wave + Local Orbitals Program for Calculating Crystal Properties* (Karlheinz Schwarz, Technische Universität Wien, Austria, 2001), ISBN .
- [26] J.C. Slater, *Quantum Theory of Molecules and Solids* (McGraw-Hill, New York, 1974).
- [27] M.D. Segall *et al.*, *J. Phys. Condens. Matter* **14**, 2717 (2002).
- [28] F. Occelli, P. Loubeyre, and R. Letoulec, *Nature Mater.* **2**, 151 (2003).
- [29] V. Brazhkin *et al.*, *Nature Mater.* **3**, 576 (2004).
- [30] A.F. Goncharov *et al.*, *Phys. Rev. B* **75**, 224114 (2007).
- [31] Y. Zhao *et al.*, *J. Mater. Res.* **17**, 3139 (2002).
- [32] A. Šimůnek and J. Vackář, *Phys. Rev. Lett.* **96**, 085501 (2006).
- [33] P.L. Potapov *et al.*, *Phys. Rev. B* **70**, 045106 (2004).